Synthesis, structure and magnetization Co_4N thin films

Mukul Gupta[1*], Seema[1], Nidhi Pandey[1], S. M. Amir[2], S. Pütter[2] and S. Mattauch[2]

[1] *UGC-DAE Consortium for Scientific Research, University Campus, Khandwa Road, Indore 452 001,India*

[2] *Forschungszentrum Jülich GmbH, Jülich Centre for Neutron Science (JCNS) at Heinz Maier-Leibnitz Zentrum (MLZ), Lichtenbergstr. 1, 85747 Garching, Germany*

[*] *Corresponding author email: mgupta@csr.res.in*

Abstract

We reviewed magnetic tetra metal nitrides - Fe_4N and Co_4N for their structure, magnetization and the thermodynamics of phase formation. Opposed to Fe_4N, the formation of a stoichiometric Co_4N turns out to be extremely difficult. A review of the literature of Co_4N compound suggest that the experimental lattice parameter (LP) was always found to be smaller than the theoretical predicted value. It can also be seen that as the substrate temperature (T_s) increases, the LP of Co_4N film decreases. In this work, we deposited Co_4N films using molecular beam epitaxy (MBE), direct current magnetron sputtering (dcMS) and high power impulse MS (HiPIMS). Films were characterized using x-ray diffraction, x-ray reflectivity and atomic force microscopy. It was found that at high T_s, N out-diffusion significantly affects the growth of Co_4N phase. We found that the MBE deposited films did not show any signature of Co_4N phase when T_s<703 K but at T_s= 703 K, the phase formed can be assigned to fcc Co rather than Co_4N. On the other hand, the dcMS and HiPIMS grown films clearly show the presence of Co_4N phase even at T_s= 300 K. Detailed analysis of Co_4N films grown using dcMS and HiPIMS reveals that HiPIMS grown films are single phase and have a denser microstructure. The density of HiPIMS deposited film was also found to be close the theoretical value. Polarized neutron reflectivity measurements were carried out to measure the magnetization. Differences in the magnetic moment have been correlated with structural parameters. Obtained results are presented and discussed in terms of involved thin film growth mechanism.

Keywords: tetra metal nitrides; cobalt nitride; reactive sputtering; high power impulse magnetron sputtering; magnetic thin films

1. Introduction

Tetra metal nitrides of Fe and Co i.e. Fe_4N and Co_4N are interesting magnetic compounds as they possess magnetic properties that are superior than their host metals. In addition, the nitriding process also inhibits the corrosion. Both Fe_4N and Co_4N have been predicted to have a half metallic character and the spin polarization ratio (SPR) of Fe_4N is predicted to be almost 100% [1], whereas for Co_4N, it could be as high as 88% [2, 3, 4]. They both have a common anti perovskite type fcc structure in which metal atoms occupy the corner and face centered positions and N atoms occupy the body centered sites as shown in fig. 1. The insertion of N atoms causes an expansion in the lattice parameter (LP) which is about 9% in Fe_4N and about 6% in Co_4N, as compared to the hypothetical fcc Fe or Co. Such an expansion leads to high volume - high magnetic moment (**M**) for the corner site FeI/CoI atoms whereas the covalent bonding between FeII/CoII and N atoms results in reduced **M** [4]. Theoretically, the values of **M** for FeI(CoI) and FeII(CoII) sites are 2.92(1.97) and 2.14(1.49) μ_B/atom, respectively. The average value of **M** for Fe_4N and Co_4N is 2.53 and 1.73 μ_B/atom, which is significantly larger than pure Fe or Co metals at 2.21 and 1.6 μ_B/atom [4]. In essence, the corrosion resistance, high SPR and high **M** makes Fe_4N and Co_4N an attractive candidate for the spintronic application and they may be considered as an alternative to Heusler alloys [5].

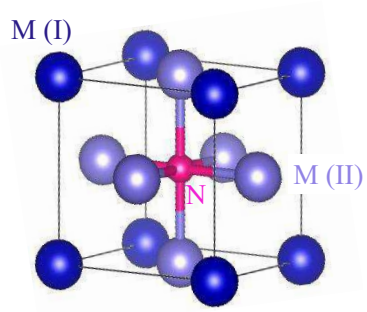

Figure 1: Schematic diagram of tetra metal nitride anti perovskite type *fcc* structure. Here M = Fe or Co have inequivalent corner or face centered sites and N atoms occupy the center position.

Recently, exchange interactions and Curie temperature (T_C) of tetra metal nitrides of Cr, Mn, Fe, Co and Ni were calculated and it was predicted that the T_C of Fe_4N and Co_4N would be 668 and 827 K, respectively [6]. These values of T_C are significantly larger than most half metal ferromagnets [5]. Combined with the fact that Fe_4N and Co_4N are environment friendly, they can be an attractive choice in spintronics. In spite of this, relatively less attention has been paid to tetra metal nitrides. In

Table 1: A survey of lattice parameters (LPs) of Co_4N thin films deposited at different substrate temperatures (T_s) using different deposition methods. The theoretical value of LP for fcc Co is 3.54 Å and for Co_4N it is 3.73 Å [3, 19].

T_s (K)	LP (Å)	Deposition Method	Reference
435	3.59	rf-sputtering	[20]
525	3.54	dc-sputtering	[21, 22, 23]
525	3.56	dc-sputtering	[24, 25]
675	3.52	MBE	[19]
725	3.52	MBE	[19]

between the two, Co_4N has has got even less attention. The reasons for this can be understood considering the thermodynamics of Fe_4N and Co_4N phase formations. The enthalpy of formation energy (ΔH_f°) for Fe_4N is about -0.9 eV and it is even larger for Co_4N at -0.03 eV (for fcc Co+N_2) or +0.05 eV (for hcp Co+N_2) [7]. These values are significantly larger than easily forming metal nitrides e.g. for TiN, ΔH_f° = -4.36 eV [8]. Therefore, inherently the formation of Fe_4N and Co_4N is difficult, more so for Co_4N as $\Delta H_f^\circ \sim 0$. Nevertheless, stoichiometric and epitaxial Fe_4N films with the LP matching to its theoretical values have been reported in several experimental works [9, 10, 11, 12, 13, 14, 15, 16, 17, 18].

However for Co_4N, even experimental realization of a stoichiometric Co_4N phase is questionable. This becomes clear by comparing the theoretically predicted and experimentally observed values of LP for Co_4N. Theoretical LP of fcc Co and Co_4N are 3.54 and 3.73Å, respectively [3, 19]. As shown in table 1, the experimentally obtained LP of Co_4N is nowhere close to its theoretical value, rather it is more close to fcc Co, specially at high T_s(≥525 K). It can also be seen from the table 1 that the LP decreases as T_s increases. Recently, N self-diffusion measurements were carried out in the Co-N system and it was found that N diffusion is significantly faster in Co-N as compared to Fe-N [26]. This suggests that when Co_4N films are deposited at high T_s N may diffuse out completely leaving behind fcc Co. This behavior was also observed in reactively sputtered Co-N films grown at T_s= 523 K [23]. However, when Co-N films were deposited at ambient temperature (at 300 K, without intentional heating) a variety of Co-N phases emerges including the Co_4N phase with its LP coming close to 3.7 Å [27, 28]. More recently, stoichiometric Co_4N epitaxial thin films were deposited on a $LaAlO_3$ (100) and MgO(100) substrates at T_s = 300 K [26] and it was found that though it is possible to grow stoichiometric and epitaxial films at 300 K, their long range ordering would not be established to its fullest in absence of sufficient adatom mobility. In addition, Co_4N films grown at T_s= 300 K, exhibited an impurity phase, probably due to co-precipitation of Co_3N phase. This can be inferred from the asymmetric peak profiles observed in the x-ray diffraction patterns by Asshara *et al*. [29] and also recently [27].

Therefore, to attain Co_4N phase with a long range crystalline ordering it is essential that the adatom mobility must be enhanced without raising the growth temperature. In recent years high power impulse magnetron sputtering (HiPIMS) has emerged as an advancement in the direct current magnetron sputtering (dcMS) technique. In this technique, high power pulses (impulse) are applied in a low duty cycle and a large fraction of the sputtered species is ionized. In addition, gases present in the vicinity of target are also ionized [30]. This is in contrast with the conventional dcMS technique where sputtered species and gases are mostly neutral. Ionized plasma has an effect on the film growth and in several cases HiPIMS deposited films exhibit a globular type growth instead of columnar type growth generally taking place in most of the thin deposition processes. The advantages of reactive HiPIMS (R-HiPIMS) process carried out in presence of a reactive gas (e.g. O_2, N_2 etc.) are even more subtle. It has been observed that target the poisoning effects (i.e. modification of target surface by reactive gas) in the R-HiPIMS can be reduced or even completely eliminated [31]. Such reduction in target poisoning is very important for growth of a stoichiometric compound. R-HiPIMS has been used to grow several nitrides e.g. TiN, CrN, ZrN, Fe-N, TaN, AlN, GaN, SiN etc. As summarized by Anders *et al*. [31], the advantages of R-HiPIMS (compared to dcMS) can be seen in terms column free growth, dense microstructure, smoother surface and interfaces and elimination of target poisoning. Therefore, it will be interesting to see the effect of R-HiPIMS process on the growth of Co_4N films.

In this work, we present the details of growth, structure and magnetic properties of Co_4N thin films deposited using dcMS, R-HiPIMS and also with molecular beam epitaxy (MBE). While dcMS and MBE have been previously used to grow Co_4N films, HiPIMS has been used for the first time in this work. In case of MBE process, samples were grown directly on a $LaAlO_3$(LAO)(111) substrate at different T_s. We found that at low T_s, the presence of Co_4N could not be seen but at high T_s films can be assigned to fcc Co rather than to a Co_4N phase. Using dcMS and R-HiPIMS processes, polycrystalline Co_4N films were grown on an amorphous quartz substrate. It was found that target poisoning effects can be reduced in the R-HiPIMS process and films are oriented along the (111) plane and they show better crystallinity as compared to films deposited using dcMS process. The magnetization of samples studied using polarized neutron reflectivity (PNR). The role of thin film growth process in affecting the microstructure and the magnetic properties of Co_4N films is presented and discussed in this work.

2. Experimental

Samples were deposited using MBE (DCA, M600 system at JCNS, Garching), dcMS and HiPIMS (ATC Orion 8, AJA Int. Inc. at UGC-DAE CSR, Indore) [32] techniques. In MBE a rf N-plasma source was used and in dcMS and HiPIMS a mixture of Ar and N_2 was used to evaporate/sputter pure Co. In all cases, a pure Co sample was also deposited as a reference. In MBE chamber the base pressure was about 5×10^{-10} mbar and with the N_2 gas flow of 0.2 standard cubic centimeter per minute (sccm) in the rf plasma source, the pressure during growth was about 1×10^{-5} mbar. Sample were grown on a $LaAlO_3$ (LAO) substrate having (111) orientation. Here LAO was used as its

lattice mismatch with Co_4N is less than 2%. Growth of sample thickness was monitored using a pre-calibrated quartz microbalance and the structure was monitored using reflection high energy electron diffraction (RHEED). Typical deposition rate for pure Co was 0.95 Å/min and for Co-N samples they were 0.85 Å/min. The substrate temperature was varied from 373 to 703 K. Total film thickness was about 200 Å.

In dcMS and HiPIMS processes the Ar to N_2 gas ratio was about 2:1 and the total gas flow was 50 sccm which increases the base pressure from 5×10^{-8} mbar to 3×10^{-3} mbar. In the dcMS process sputtering power was about 150 W and in the HiPIMS the average power was about 250 W but the peak power was about 6 kW, with a pulse duration 90 μs and frequency of 500 Hz, yielding a duty cycle of 4.5%. In both cases the same Co target (diameter 3 inch, thickness 0.125 inch, purity 99.95%) was used. Prior to deposition, substrates were heated at about 500 K for couple of hours and then cooled down to either 358 or 300 K. The substrates were rotated at 60 rpm for better uniformity. All other deposition parameters were kept identical for the dcMS and HiPIMS processes. For each case two sets of samples were deposited on amorphous quartz (SiO_2) and Si substrates - one with a thickness of about 500 and other about 1500 Å. Thicker samples were used for x-ray diffraction (XRD) and atomic force microscopy (AFM) measurements, while x-ray reflectivity and polarized neutron reflectivity measurements were carried out on both samples.

Samples were characterized with XRD (Bruker D8 Advance), XRR (Bruker D8 Discover) using Cu K-α x-rays. The microstructure of samples was measured using AFM in the non-contact mode. The MAgnetic Reflectometer with high Incident Angle (MARIA) of the JCNS, Garching, Germany was used for PNR in the horizontal scattering plane geometry [33]. During PNR measurements a magnetic field of about 0.5 Tesla was applied to saturate the sample magnetically and they were fitted using GenX software [34].

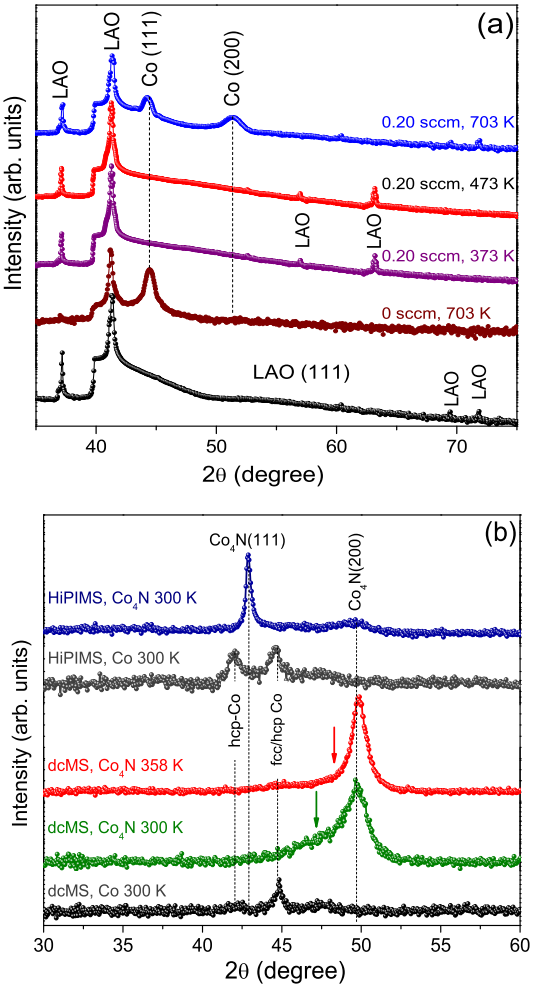

Figure 2: X-ray diffraction patterns of Co-N films deposited using MBE on a LaAlO3 (111) substrate (a) and with dcMS and HiPIMS on an amorphous quartz substrate (b). Growth conditions (process gas flow and/or substrate temperature) are mentioned in each case.

3. Results and Discussion

3.1. Structure and Morphology

Fig. 2 (a) shows the XRD patterns of samples deposited using MBE on a LAO(111) substrate. The XRD pattern of bare LAO(111) substrate has also been shown there. It can be seen that the sample deposited at T_s= 703 K (without N_2 gas flow in the rf plasma source), shows reflection corresponding to fcc Co(111) and the lattice parameter (LP) comes out to be about 3.54 Å, as expected for fcc Co [3, 19]. Similarly for the sample deposited using N_2 gas flow (0.2 sccm), this peak position is slightly shifted to lower 2θ value yielding LP = 3.56 Å. This value is consistent with earlier works where Co_4N phase has been claimed at similar growth temperatures [19]. In addition, the reflection corresponding to fcc Co(200) can also be seen. At lower T_s, no peaks (other than LAO substrate) can be seen. It appears that when T_s<703 K the long range ordering has not established signifying the growth of a disordered structure. At 703 K only fcc Co grows which may have a small amount of N at the interstitial sites causing a slight expansion in the LP from 3.54 to 3.56 Å. This may happen if N diffuses out during growth itself leaving behind fcc Co.

Fig.2 (b) shows XRD patterns of samples deposited using dcMS and HiPIMS. When deposited without N_2 gas flow, both films show reflections corresponding to fcc/hcp Co, which are generally observed in sputtered Co thin films [23, 27]. Reactively sputtered samples, both with dcMS and HiPIMS show reflections corresponding to Co_4N. For the sample grown with dcMS at 300 K, Co_4N(200) reflection is prominent. As the T_s is raised slightly to 358 K, this peak shifts to higher 2θ signifying that the LP decrease from 3.67 (at 300 K) to 3.65 Å (at 358 K). In agreement with our earlier observation about N self-diffusion measurements [26], N starts to diffuse out even when the T_s is raised marginally. In fact at 523 K, N diffuses out completely leaving behind fcc Co, even in the case when only N_2 was used as the sputtering gas [23]. This also explains the absence of Co_4N phase in the MBE grown samples.

The XRD peak profiles in dcMS deposited Co_4N samples show an asymmetry, probably due to precipitation of Co_3N phase (marked by an arrow). The sample grown by HiPIMS shows

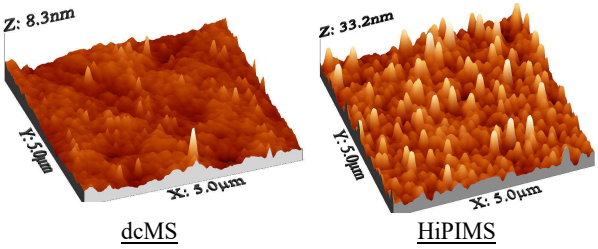

Figure 3: AFM images of Co_4N samples grown using dcMS and HiPIMS processes at T_s= 300 K.

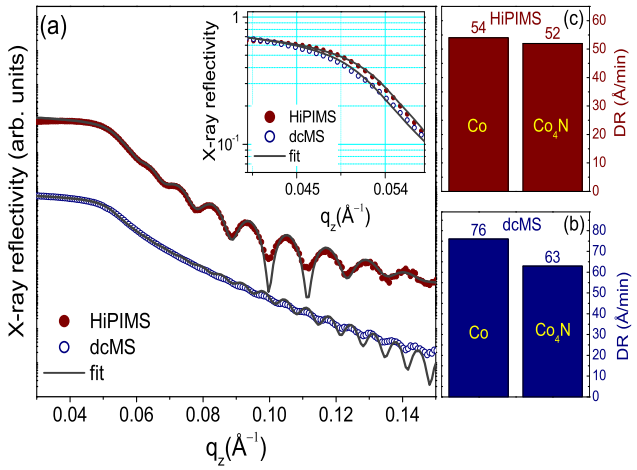

Figure 4: X-ray reflectivity pattern of Co_4N films deposited using dcMS and HiPIMS (a). The inset of (a) compares the critical angle region depicting the change in the density of Co_4N thin films grown by dcMS and HiPIMS. A comparison of deposition rate (DR) for pure Co metal and Co_4N is shown in (b) for dcMS and in (c) for the samples grown using HiPIMS.

a strong Co_4N(111) reflection along with a weak Co_4N(200) hump. However, no asymmetry arising from Co_3N or any other Co-N phase can be seen. It may be noted that such asymmetric peak profiles in Co_4N films deposited with out any intentional heating was also seen in earlier works [27, 29]. The The grain size calculated from the peak widths comes out to be 5 and 15 nm for the Co_4N sample deposited at 300 K with dcMS and HiPIMS processes, respectively. Clearly, the HiPIMS grown films are superior in terms of crystalline qualities. The LP of Co_4N films grown by dcMS and HiPIMS at T_s= 300 K is 3.67 and 3.66 Å, these values are only about 2% smaller than the theoretical value of 3.73 Å expected for Co_4N.

In order to further investigate the differences in the morphology of Co_4N films grown with dcMS and HiPIMS, AFM measurements were carried out as shown in fig. 3. Here, we can see that dcMS films are featureless, whereas HiPIMS grown films show well-distributed grains. From our XRD measurements also we find that the grain size increases by a about a factor of three, AFM results further support this.

3.2. Deposition Rates and Density

We did x-ray reflectivity (XRR) measurements to measure thickness, roughness and density of samples deposited using dcMS and HiPIMS processes. Experimental and fitted XRR patterns are shown in fig. 4 (a). Fitting was done using Parratt32 software [35] based on Parratt's formulism [36]. The thickness of films deposited using dcMS and HiPIMS were about 800 and 500 Å, respectively. Typical roughness was about 15 Å in both cases. As shown in the inset of fig. 4 (a), the critical angle of HiPIMS deposited film occurs at a significantly higher q_z than that of dcMS sample. This indicated that the density of HiPIMS deposited films will be higher. From the fitting of XRR data we found that the density of dcMS and HiPIMS samples comes out to be 7.6 and 8.05 gcm^{-3}. Theoretical density of Co_4N is 8.1 gcm^{-3} [37] and its closeness with the HiPIMS deposited film signifies that the film deposited using HiPIMS is stoichiometric Co_4N. It may be noted that estimation of density with XRR may typically have intrinsic errors (due to alignment etc.) of about 5%, but even after considering this, the density of HiPIMS deposited film is indeed high.

From the known deposition times and measuring the film thickness, we calculated the deposition rate (DR). We found that DR was 76 and 63 Å for Co and Co_4N films grown with the dcMS and 54 and 52 Å for the films grown with the HiPIMS process as shown schematically in fig. 4 (b) and (c), respectively for dcMS and HiPIMS samples. Though the overall DRs are low in the HiPIMS process (due to low duty cycle), the reduction in rate compared to pure Co metal is far greater in the dcMS process. It is known that the DR in a reactive sputtering process generally reduces (compared to pure metal) due to a compound formation taking place at the target itself, known as target poisoning. We notice that this reduction in DR was about 17% in the dcMS and only about 4% in the HiPIMS process. It is known that target poisoning can be completely or partially suppressed in the R-HiPIMS process [38] and can be understood by rarefaction of the reactive gas in the vicinity of the target [39]. As the DR are comparable for Co and Co_4N films in the HiPIMS processes, it can be anticipated that the growth of Co_4N film takes places from the metallic state of the target. On the other hand, in the dcMS process, Co_4N emerges out the transient state of the target which is not so well defined. Formation of a compound from the transient state of a target may not be reproducible. Reduction of target poisoning therefore is an important criteria to grow stoichiometric thin films in a reactive sputtering process.

3.3. Influence of film growth kinetics on stoichiometry

Combining XRD, XRR and AFM measurements, it can be concluded that the HiPIMS deposited film is stoichiometric Co_4N. Observed results on the growth behavior of Co_4N thin films can be understood considering the kinetics of film growth involved in the processes. In case of MBE, the adatom energies are typically about a fraction of an eV, whereas in sputtering they are typically tens of eV. In absence of any temperature assistance,

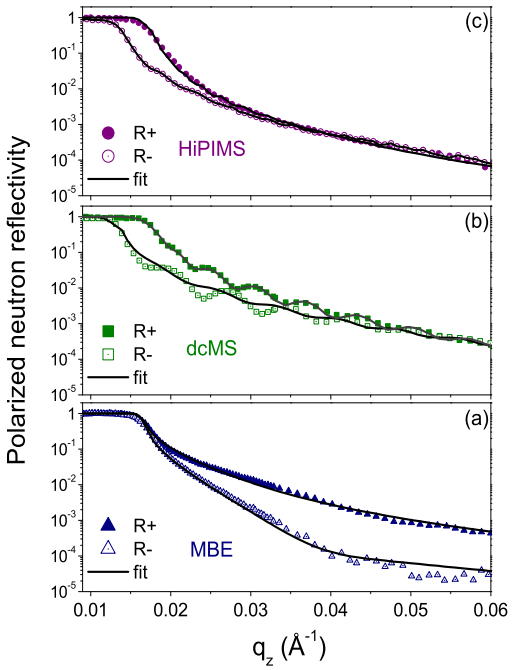

Figure 5: Polarized neutron reflectivity patterns for samples grown using MBE (a) dcMS (b) and HiPIMS (c).

the adatom mobility in the MBE process in not sufficient to establish the crystalline order. On the other hand in the sputtering process higher adatom energies lead to high mobility which can lead to formation of Co_4N phase. However, in the HiPIMS process the ionization of both metal and reactive gas atoms results in further enhancement in adatom mobility resulting in better crystalline order. In addition, such ionization may also alter the thermodynamical constraints so that single phase and stoichiometric Co_4N get formed in the HiPIMS process. Moreover, since the formation of Co_4N phase takes place from the metallic state of the target in HiPIMS, the probability for formation of a stoichiometric compound becomes higher.

3.4. Magnetic Properties

It will be interesting to compare the magnetization of these films. It is well-known that PNR is the best technique to measure the magnetization and the magnetic depth profiles [40]. Since in this technique contributions to magnetization coming from the surface regions, bulk of the sample and the film-substrate interfaces can be probed individually. We did PNR measurements on samples deposited with MBE, dcMS and HiPIMS processes and they are shown in fig. 5 (a), (b) and (c), respectively.

Here, the MBE sample was deposited at T_s= 703 K, while those with dcMS and HiPIMS at 300 K. It may be noted that the neutron scattering lengths (SL) for Co and N are 2.3 and 9.36 fm [41] and therefore, the neutron scattering length density (SLD), a product of SL and number density will increase as N is added in Co. It may be noted that the SLD of LAO is 6×10^{-6} Å^{-2} and that of quartz (SiO_2) is 3.47×10^{-6} Å^{-2}. As the SLD of substrate and that film are comparable in LAO, the difference between spin up and down reflectivities (R^+,R^-) will be very small when the sample is deposited on a LAO substrate. Also, the R^- will be influenced by the substrate only.

It is known that in PNR, the contributions from the nuclear (structural) and magnetic SLD appear together and they can not be individually separated unless one of the quantities is known a priori. Since from our XRR measurements the information about structural (nuclear) density was already known, to fit the PNR patterns, we used this as an input and kept it fixed so that the magnetic contribution can be estimated accurately. Fitted PNR patterns (using GenX software [34]) are also shown in fig. 5. From the fitting the magnetic moment **M** comes out to be 1.6, 1.52 and 1.55μ_B/Co atom for samples deposited using MBE, dcMS and HiPIMS, respectively. The values for MBE grown sample match well with the theoretical value of Co, however for the dcMS and HiPIMS samples they are smaller than than the theoretical value Co_4N at bout 1.73μ_B/Co. Here, it may be noted that even in HiPIMS deposited sample the LP at 3.66 Å is still smaller than the theoretical LP of 3.73 Å. It can be foreseen that further optimization such as by increasing the peak power, the ionization of reactive gas and sputtered adatoms can be enhanced. It may be then possible to match the theoretical LP and magnetic moment in Co_4N films even for polycrystalline samples. It is further emphasized that since it is not possible to raise the substrate temperature during the growth of Co_4N phase, additional parameters leading to increased adatom mobility might be the key to sustain the long range ordering during the growth of Co_4N thin films.

4. Conclusion

In conclusion, in this work we presented a review of tetra iron and cobalt nitrides - Fe_4N and Co_4N. Due to smaller enthalpy of formation and smaller N out-diffusion, it is rather convenient to get a stoichiometric Fe_4N phase at high substrate temperature. However, the growth of stoichiometric Co_4N is more challenging as even a slight increase in substrate temperature leads to N deficiency. In absence of sufficient adatom mobility that can be easily accessed by raising the temperature, alternate methods are required to achieve this. In this work, we demonstrated that by utilizing the ionized plasma in the HiPIMS process the crystalline quality and the density of Co_4N films can be increased to a great extent. In our HiPIMS grown Co_4N film, the lattice parameter and density was only about 2% smaller than the theoretical values but even then the magnetic moment was about 10% smaller. It can be anticipated that by further optimizing the growth conditions in the HiPIMS process fully stoichiometric films Co_4N films can be grown which may have larger than Co magnetic moment, as expected theoretically.

Acknowledgments

We would like to thank to the Department of Science and Technology, India (SR/NM/Z-07/2015) for the financial sup-

port and Jawaharlal Nehru Centre for Advanced Scientific Research (JNCASR) for managing the project. This project has received funding from the EU H2020 research and innovation programme under grant agreement No 654360 having benefitted from the access provided by Jülich Centre for Neutron Science (JCNS) in Garching within the framework of the NFFA-Europe Transnational Access Activity proposal ID600. We acknowledge the help received from Layanta Behera in sample preparation and XRD measurements, A. Gome and V. R. Reddy in XRR measurements and M. Gangrade and V. Ganesan in AFM measurements. We are thankful to V. Ganesan and A. K. Sinha for support and encouragements.

References

[1] S. Kokado, N. Fujima, K. Harigaya, H. Shimizu, A. Sakuma, Phys. Rev. B 73 (2006) 172410.
[2] Y. Takahashi, Y. Imai, T. Kumagai, Journal of Magnetism and Magnetic Materials 323 (2011) 2941 – 2944.
[3] S. F. Matar, A. Houari, M. A. Belkhir, Phys. Rev. B 75 (2007) 245109.
[4] A. Houari, S. F. Matar, M. A. Belkhir, Journal of Magnetism and Magnetic Materials 322 (2010) 658 – 660.
[5] H. Li, X. Li, D. Kim, G. Zhao, D. Zhang, Z. Diao, T. Chen, J.-P. Wang, Applied Physics Letters 112 (2018) 162407.
[6] M. Meinert, Journal of Physics: Condensed Matter 28 (2016) 056006.
[7] Y. Imai, M. Sohma, T. Suemasu, Journal of Alloys and Compounds 611 (2014) 440 – 445.
[8] B. Saha, A. Shakouri, T. D. Sands, Applied Physics Reviews 5 (2018) 021101.
[9] H. Chatbi, M. Vergnat, P. Bauer, G. Marchal, Applied Physics Letters 67 (1995) 430–432.
[10] J. M. Gallego, S. Y. Grachev, D. M. Borsa, D. O. Boerma, D. Écija, R. Miranda, Phys. Rev. B 70 (2004) 115417.
[11] J. L. Costa-Krämer, D. M. Borsa, J. M. García-Martín, M. S. Martín-González, D. O. Boerma, F. Briones, Phys. Rev. B 69 (2004) 144402.
[12] S. Atiq, H.-S. Ko, S. A. Siddiqi, S.-C. Shin, Applied Physics Letters 92 (2008) –.
[13] E. L. P. y. Blancá, J. Desimoni, N. E. Christensen, H. Emmerich, S. Cottenier, physica status solidi (b) 246 (2009) 909–928.
[14] K. Ito, K. Harada, K. Toko, M. Ye, A. Kimura, Y. Takeda, Y. Saitoh, H. Akinaga, T. Suemasu, Applied Physics Letters 99 (2011) –.
[15] I. Dirba, M. B. Yazdi, A. Radetinac, P. Komissinskiy, S. Flege, O. Gutfleisch, L. Alff, Journal of Magnetism and Magnetic Materials 379 (2015) 151 – 155.
[16] M. Naito, K. Uehara, R. Takeda, Y. Taniyasu, H. Yamamoto, Journal of Crystal Growth 415 (2015) 36 – 40.
[17] D. Glden, E. Hildebrandt, L. Alff, Journal of Magnetism and Magnetic Materials 422 (2017) 407 – 411.
[18] Q. Lu, M. Xie, G. Han, B. Zheng, Y. Song, J. Qiang, X. Wang, Z. Wu, P. Yan, W. Liu, Journal of Magnetism and Magnetic Materials 474 (2019) 76 – 82.
[19] K. Ito, K. Harada, K. Toko, H. Akinaga, T. Suemasu, Journal of Crystal Growth 336 (2011) 40 – 43.
[20] K. Oda, T. Yoshio, K. Oda, Journal of Materials Science 22 (1987) 2729–2733.
[21] A. Costa, R. da Silva, L. Ferreira, M. Carvalho, C. Silva, N. Franco, M. Godinho, M. Cruz, Journal of Magnetism and Magnetic Materials 350 (2014) 129 – 134.
[22] C. Silva, A. Vovk, R. da Silva, P. Strichonavec, P. Algarabel, A. Casaca, C. Meneghini, I. Carlomagno, M. Godinho, M. Cruz, Journal of Alloys and Compounds 633 (2015) 470 – 478.
[23] N. Pandey, M. Gupta, R. Gupta, S. Chakravarty, N. Shukla, A. Devishvili, Journal of Alloys and Compounds 694 (2017) 1209 – 1213.
[24] X. Wang, H. Jia, W. Zheng, Y. Chen, S. Feng, Thin Solid Films 517 (2009) 4419 – 4424.
[25] K. Ito, K. Kabara, T. Sanai, K. Toko, Y. Imai, M. Tsunoda, T. Suemasu, Journal of Applied Physics 116 (2014) –.
[26] N. Pandey, M. Gupta, R. Gupta, Z. Hussain, V. R. Reddy, D. M. Phase, J. Stahn (2019).
[27] R. Gupta, N. Pandey, A. Tayal, M. Gupta, AIP Advances 5 (2015) 097131.
[28] N. Pandey, M. Gupta, R. Gupta, P. Rajput, J. Stahn, Journal of Magnetism and Magnetic Materials 448 (2018) 274 – 277.
[29] H. Asahara, T. Migita, T. Tanaka, K. Kawabata, Vacuum 62 (2001) 293 – 296.
[30] J. T. Gudmundsson, N. Brenning, D. Lundin, U. Helmersson, Journal of Vacuum Science and Technology A 30 (2012) –.
[31] A. Anders, Journal of Applied Physics 121 (2017) 171101.
[32] A. Tayal, M. Gupta, A. Gupta, V. Ganesan, L. Behera, S. Singh, S. Basu, Surface and Coatings Technology 1 (2015) 2.
[33] S. Mattauch, A. Koutsioubas, U. Rücker, D. Korolkov, V. Fracassi, J. Daemen, R. Schmitz, K. Bussmann, F. Suxdorf, M. Wagener, P. Kämmerling, H. Kleines, L. Fleischhauer-Fuß, M. Bednareck, V. Ossoviy, A. Nebel, P. Stronciwilk, S. Staringer, M. Gödel, A. Richter, H. Kusche, T. Kohnke, A. Ioffe, E. Babcock, Z. Salhi, T. Bruckel, Journal of Applied Crystallography 51 (2018) 646–654.
[34] M. Björck, G. Andersson, Journal of Applied Crystallography 40 (2007) 1174–1178.
[35] C. Braun, Parratt32- The Reflectivity Tool, HMI Berlin, 1997-99.
[36] L. G. Parratt, Phys. Rev. 95 (1954) 359.
[37] Journal of Alloys and Compounds 633 (2015) 470 – 478.
[38] M. Hala, N. Viau, O. Zabeida, J. E. Klemberg-Sapieha, L. Martinu, Journal of Applied Physics 107 (2010) 043305.
[39] E. Wallin, U. Helmersson, Thin Solid Films 516 (2008) 6398 – 6401.
[40] S. Hope, J. Lee, P. Rosenbusch, G. Lauhoff, J. A. C. Bland, A. Ercole, D. Bucknall, J. Penfold, H. J. Lauter, V. Lauter, R. Cubitt, Phys. Rev. B 55 (1997) 11422.
[41] J. Dawidowski, J. R. Granada, J. R. Santisteban, F. Cantargi, L. A. R. Palomino 44 (2013) 471 – 528.